Original Article

MOLECULAR METABOLISM

Dual role of protein tyrosine phosphatase 1B in the progression and reversion of non-alcoholic steatohepatitis

Águeda González-Rodríguez [1,2,*,9], M. Pilar Valdecantos [3,4,9], Patricia Rada [3,4], Annalisa Addante [5], Inés Barahona [3,4], Esther Rey [1,2], Virginia Pardo [3,4], Laura Ruiz [3,4], Laura M. Laiglesia [6], María J. Moreno-Aliaga [6,7,8], Carmelo García-Monzón [1,2], Aránzazu Sánchez [5], Ángela M. Valverde [3,4,**]

ABSTRACT

Objectives: Non-alcoholic fatty liver disease (NAFLD) is the most common chronic liver disease in Western countries. Protein tyrosine phosphatase 1B (PTP1B), a negative modulator of insulin and cytokine signaling, is a therapeutic target for type 2 diabetes and obesity. We investigated the impact of PTP1B deficiency during NAFLD, particularly in non-alcoholic steatohepatitis (NASH).

Methods: NASH features were evaluated in livers from wild-type (PTP1BWT) and PTP1B-deficient (PTP1BKO) mice fed methionine/choline-deficient diet (MCD) for 8 weeks. A recovery model was established by replacing MCD to chow diet (CHD) for 2–7 days. Non-parenchymal liver cells (NPCs) were analyzed by flow cytometry. Oval cells markers were measured in human and mouse livers with NASH, and in oval cells from PTP1BWT and PTP1BKO mice.

Results: PTP1BWT mice fed MCD for 8 weeks exhibited NASH, NPCs infiltration, and elevated *Fgf21*, *Il6* and *Il1b* mRNAs. These parameters decreased after switching to CHD. PTP1B deficiency accelerated MCD-induced NASH. Conversely, after switching to CHD, PTP1BKO mice rapidly reverted NASH compared to PTP1BWT mice in parallel to the normalization of serum triglycerides (TG) levels. Among NPCs, a drop in cytotoxic natural killer T (NKT) subpopulation was detected in PTP1BKO livers during recovery, and in these conditions M2 macrophage markers were up-regulated. Oval cells markers (EpCAM and cytokeratin 19) significantly increased during NASH only in PTP1B-deficient livers. HGF-mediated signaling and proliferative capacity were enhanced in PTP1BKO oval cells. In NASH patients, oval cells markers were also elevated.

Conclusions: PTP1B elicits a dual role in NASH progression and reversion. Additionally, our results support a new role for PTP1B in oval cell proliferation during NAFLD.

Keywords PTP1B; Steatosis; Steatohepatitis; Inflammation; Oval cells

1. INTRODUCTION

Protein tyrosine phosphatase 1B (PTP1B) has emerged as a major negative regulator of insulin and leptin sensitivity, acting by dephosphorylation of the insulin receptor (IR) and leptin receptor-associated Janus kinase 2 (JAK2), respectively [1,2]. PTP1B inhibition has been proposed as a promising drug target for type 2 diabetes mellitus (T2DM) and obesity since its deficiency in mice enhanced insulin sensitivity and conferred resistance to diet-induced obesity [3,4]. Regarding hepatic homeostasis, the importance of PTP1B in various

[1]Hospital Universitario Santa Cristina, Instituto de Investigación Sanitaria Princesa, 28009 Madrid, Spain [2]Centro de Investigación Biomédica en Red de Enfermedades Hepáticas y Digestivas (CIBERehd), Instituto de Salud Carlos III, 28029 Madrid, Spain [3]Instituto de Investigaciones Biomédicas Alberto Sols (Centro Mixto CSIC-UAM), Arturo Duperier 4, 28029 Madrid, Spain [4]Centro de Investigación Biomédica en Red de Diabetes y Enfermedades Metabólicas Asociadas (CIBERdem), Instituto de Salud Carlos IIII, 28029 Madrid, Spain [5]Departamento de Bioquímica y Biología Molecular II, Facultad de Farmacia, Universidad Complutense, Instituto de Investigación Sanitaria del Hospital Clínico San Carlos (IdISSC), 28040 Madrid, Spain [6]Departmento de Nutrición, Ciencias de la Alimentación y Fisiología/Centro de Investigación en Nutrición, Universidad de Navarra, 31008 Pamplona, Spain [7]Centro de Investigación Biomédica en Red de la Fisiopatología de la Obesidad y Nutrición (CIBERobn), Instituto de Salud Carlos III, 28029 Madrid, Spain [8]Instituto de Investigación Sanitaria de Navarra (IdiSNA), Pamplona, Spain

[9] Equal contributors.

*Corresponding author. Hospital Universitario Santa Cristina, Instituto de Investigación Sanitaria Princesa, 28009 Madrid, Spain. Fax: +34 915854401. E-mail: aguedagr.phd@gmail.com (Á. González-Rodríguez).

**Corresponding author. Instituto de Investigaciones Biomédicas Alberto Sols (Centro Mixto CSIC-UAM), Arturo Duperier 4, 28029 Madrid, Spain. E-mail: avalverde@iib.uam.es (Á.M. Valverde).

Abbreviations: mRNA, messenger RNA; Fgf21, fibroblast growth factor 21; Cd36, fatty acid translocase; IL1β, Interleukin 1β; IL6, Interleukin 6; Ccl2, chemokine (C–C motif) ligand 2; IL4, Interleukin 4; IL13, Interleukin 13; Arg1, arginase 1; No2, inducible nitric oxide synthase; TNFα, tumor necrosis factor α

Received September 12, 2017 • Revision received October 19, 2017 • Accepted October 22, 2017 • Available online 31 October 2017

https://doi.org/10.1016/j.molmet.2017.10.008

cellular processes such as insulin resistance [5,6], lipogenesis [7], and the balance between death and survival in hepatocytes [8,9] has been extensively studied. Global PTP1B deficiency protects from hepatic steatosis and improves hepatic regeneration in mice fed high fat diet (HFD) [10]. Likewise, hepatocyte-specific PTP1B-deficient mice presented improved glucose and lipid homeostasis, in part by reduction of hepatic endoplasmic reticulum (ER) stress markers induced by HFD feeding [7]. On the other hand, PTP1B is also a key modulator in immune cell signaling that controls cytokine-mediated signaling pathways by dephosphorylation of JAK2, the non-receptor tyrosine-protein kinase 2 (TYK2), and signal transducer and activators of transcription 5 and 6 (STAT5 and STAT6) [11–13]. These studies shed light of a dual role of PTP1B in metabolic diseases though its different actions in non-immune and immune cells.

Non-alcoholic fatty liver disease (NAFLD) is considered the hepatic manifestation of the metabolic syndrome since it is strongly associated with obesity, insulin resistance, T2DM, and cardiovascular complications [14]. Due to the increase in the incidence of metabolic syndrome, NAFLD has become the most frequent chronic liver disease in Western countries, therefore representing an important public health problem [15]. At a molecular level, the hypothesis describing the molecular mechanisms involved in NAFLD progression was proposed by Day et al. [16] and is known as the "Two Hit Hypothesis". The presence of fat in >5% of hepatocytes [17] is considered the first hit. The second "impact" involves inflammation, necrosis, and activation of the fibrogenic cascade, which leads to non-alcoholic steatohepatitis (NASH) characterized by a robust proinflammatory component in the hepatic tissue, as well as by hepatocyte ballooning. NASH can progress to more severe and irreversible stages of the disease such as fibrosis and cirrhosis [16]. Thus, elucidation of the molecular mechanisms involved in disease progression is urgently needed to identify new targets and implement efficient therapies. In this regard, the role of PTP1B during the progression of NAFLD beyond simple steatosis (fatty liver) and particularly in the NASH stage, where lipid overloaded hepatocytes coexist with activation of non-parenchymal immune cells (NPCs) [18], remains poorly characterized.

NAFLD progresses to NASH when adaptive mechanisms that protect hepatocytes from fatty acid-mediated lipotoxicity become overwhelmed, and the ratio of hepatocyte death/regeneration becomes unbalanced. Self-renewal of hepatocytes is the main mechanism responsible for the maintenance of liver mass homeostasis after an acute liver injury. However, in conditions of chronic liver damage, this capacity for self-renewal is exhausted leading to an insufficiency in liver function. In those conditions, adult hepatic progenitor cells (HPCs), accounting for 1–3% of total liver cell pool, which could derive from normally quiescent true stem cell that reside in the biliary tree, are able to actively proliferate [19,20]. HPCs are called oval cells in rodents because of their ovoid nucleus appearance [21] and constitute a heterogenic population. They are bipotential progenitor cells that are able to differentiate towards mature hepatocytes and cholangiocytes. Thus, they represent a reserve compartment that is activated only when the mature epithelial cells of the liver are continuously damaged or inhibited in their replication or in cases of severe cell loss [22]. Therefore, oval cells plasticity, repopulation capacity and differentiation potential keep high expectations for clinical strategies aimed to improve regeneration in chronic liver diseases including NAFLD.

A commonly used nutritional model of NASH is feeding mice a methionine/choline deficient (MCD) diet that induces hepatic steatosis, focal inflammation, hepatocyte necrosis, and fibrosis [23]. These histological changes occur rapidly and are morphologically similar to those observed in human NASH [24], but the use of MCD model for preclinical studies has been debated because of the induction of body weight loss [25] in favor of the use of dietary intervention models of NASH accompanied by weight gain, insulin resistance, and other metabolic changes [26]. However, as PTP1B-deficient mice do not develop hepatic steatosis and other metabolic disorders either on a HFD [10] or during aging [27], the direct role of this phosphatase in NAFLD development, specifically in the progression towards NASH, is difficult to evaluate in diet-induced obesity models. On that basis, the aim of this study was first to determine the impact of PTP1B deficiency in NASH evolution and regression using the MCD dietary challenge as a non-obese model of NASH and, second, to unravel an unknown role of PTP1B in the dynamics of oval cells proliferation during this stage of NAFLD.

2. EXPERIMENTAL PROCEDURES

2.1. Animals and diets

All animal experimentation was conducted in accordance with Spanish and European legislation and approved by the CSIC and Comunidad de Madrid Animal Care and Use Committee. Wild-type (PTP1BWT) and PTP1B-deficient (PTP1BKO) mice were previously described [4,27]. Mice used in this study were maintained on the same mixed genetic background (C57Bl/6 J × 129 Sv/J), in light/dark (12 h light/12 h dark), temperature- (22 °C) and humidity-controlled rooms, fed with standard chow diet ad libitum, and had free access to drinking water at the animal facilities of the Instituto de Investigaciones Biomédicas Alberto Sols (CSIC-UAM, Madrid). Male animals at the age of 10–12 weeks were divided in 6 experimental groups. Mice were fed either chow diet (CHD; SAFE A04-10 Panlab, Barcelona, Spain) or MCD (TD-90262 Harland-Tecklad, Indianapolis, IN, USA) for 4 (4wMCD) or 8 weeks (8wMCD). Then, 3 groups of mice fed MCD for 8 weeks were switched to CHD for 2 (8wMCD+2dCHD), 4 (8wMCD+4dCHD) or 7 days (8wMCD+7dCHD). Daily body weight and food intake were manually measured. At the end of the experiments, animals were sacrificed and tissues were removed, weighed, and frozen at −80 °C or fixed with 4% paraformaldehyde for further analysis.

2.2. Histopathology assessment

Paraffin-embedded liver biopsy sections (5 μm) were stained with Hematoxylin & Eosin and Masson's trichrome solution and evaluated by a single blinded hepatopathologist. All liver sections measured >1.5 cm in length and showed more than 10 complete portal tracts. The percentage of hepatocytes containing lipid droplets was determined for each 10x field. An average percentage of steatosis was then determined for the entire specimen. Steatosis was assessed as outlined by Kleiner et al. [28] grading percentage involvement by steatotic hepatocytes as follows: grade 0, <5%; grade 1, 5–33%; grade 2, >33–66%; and grade 3, >66%. In addition, Brunt's histological scoring system was used to evaluate the degree of hepatocellular ballooning and lobular inflammation (grade of activity) as well as the stage of fibrosis [29].

2.3. Determination of serum transaminase levels

Serum ALT activity was determined using Reflotron strips (Roche Diagnostics, Barcelona, Spain), accordingly with the manual instructions.

2.4. Determination of triglyceride content

Hepatic lipids were extracted as previously described [30]. After purification, lipids were resuspended in isopropyl alcohol and triglycerides were analyzed with a colorimetric kit (Biosystems, Spain).

2.5. Patients

This study comprised 49 nondiabetic patients with a clinical diagnosis of NAFLD (NAFL and NASH) who underwent a liver biopsy by a percutaneous route during programmed cholecystectomy. This study was performed in agreement with the Declaration of Helsinki, and with local and national laws. The Institution's Human Ethics Committee approved the study procedures, and written informed consent was obtained from all patients before inclusion in the study (see Gonzalez-Rodriguez et al., 2014 [31] for details).

2.6. Immunohistochemistry of liver samples

Liver sections (5 μm) were immunostained for Ki67 (1:200; M7240, Dako, Glostrup, Denmark) or cytokeratin 19 (CK19) (TROMA III monoclonal antibody, Developmental Studies Hybridoma Bank, University of Iowa), using the indirect peroxidase method as described by the manufacturer.

2.7. Quantitative real-time PCR analysis

Total RNA was extracted with Trizol® reagent (Invitrogen, Madrid, Spain) and reverse transcribed using a SuperScript™ III First-Strand Synthesis System for qPCR following the manufacturer's indications (Invitrogen). qPCR was performed with an ABI 7900 sequence detector. Primer-probe sets for mouse *Cd36*, *Il6*, *Il1b*, *Tnfa*, *Ccl2*, *Il4*, *Il10*, *Arg1*, *Krt19*, *Epcam*, *Fgf21*, and *18s,* and for human *Krt19*, *Epcam*, and *18s* were purchased as predesigned TaqMan gene expression assays (Applied Biosystems, Foster City, CA, USA).

2.8. Isolation and analysis of non-parenchymal liver cells by flow cytometry

Non-parenchymal liver cells (NPCs) were isolated as previously described with slight modifications [32]. Cells ($0.3-0.5 \times 10^6$ cells/test) were incubated with CD45-FITC (rat IgG, Beckman Coulter, Madrid, Spain), CD11b-(Mac1)-PECy7 (rat IgG2bk anti-mouse, eBioscience, ThermoFisher Scientific, Waltham, MA, USA), F4/80-APC (rat IgG2ak, eBioscience), Ly6G-PE (rat IgG2ak, Pharmingen, San José, CA, USA), CD3-PECy7 (Hamster IgG, eBioscience), NK1.1-APC (mice IgG2ak anti-mouse, Pharmingen), CD8a-PE (2.4G2, Cultek, Madrid Spain), F4/80-PE (rat IgG2ak, eBioscience), Ly6C-FITC (rat IgMk, anti-mouse, Pharmingen), and CCR2-APC (rat IgG2B, R&D Systems, Minneapolis, MN, USA) or their corresponding isotype controls for 20 min at room temperature. Flow cytometry data were acquired with a FACSCanto II (BD Biosciences, Madrid, Spain) and data analysis was performed using Cytomics FC500 with the CXP program.

2.9. Hepatocyte culture and procedures

Immortalized hepatocytes were generated from wild-type and PTP1B-deficient mice as previously described [8] and were grown in Dulbecco's modified Eagle's Medium (DMEM) supplemented with 10% fetal bovine serum (FBS), antibiotics (100 U/ml penicillin and 100 μg/ml streptomycin), and 2 mM L-glutamine at 37 °C in a humidified atmosphere with 5% CO_2. For Nile Red staining, hepatocytes were fixed in paraformaldehyde (4%) and resuspended in Nile Red working solution (0.4 μg/ml). The fluorescence was determined using a FACScan flow cytometer (BD Biosciences). For bromopalmitate uptake analysis, confluent wild-type and PTP1B-deficient hepatocytes were washed with PBS and incubated for 50 min in Krebs–Ringer buffer without glucose, containing 125 mM NaCl, 5 mM KCl, 2 mM $CaCl_2$, 1.25 mM KH_2PO_4, 1.25 mM $MgSO_4.7H_2O$, 25 mM $NaHCO_3$ pH 7.4, 3% fatty acid-free bovine serum albumin (BSA), and saturated oxygen. At the end of the incubation, 1 mM (final concentration) L-carnitine (Sigma–Aldrich, Saint Louis, MO, USA), 80 μM PA (Sigma–Aldrich), and 20 μM ^{14}C-palmitic acid (58 μCi/μmol, Perkin Elmer, Waltham, MA) were added for a further 10 min. Then, cells were washed with PBS and scraped in cold buffer (0.25 M sucrose, 10 mM Tris HCl, 1 mM EDTA, and 1 mM dithiothreitol, pH 7.4). After two cycles of freezing/thawing in liquid nitrogen, radioactivity was counted in a Wallac 1409 counter (EG&G Company, USA). Results were normalized to total protein content of cell extracts and expressed as nmol/mg protein.

2.10. Macrophage culture and procedures

Peritoneal macrophages isolated from wild-type and PTP1B-deficient mice as previously described [33] were used for *in vitro* experiments and were cultured with RPMI 1640 medium supplemented with 10% heat-inactivated fetal calf serum (FCS) and antibiotics (100 U/ml penicillin, 100 μg/ml streptomycin) at 37 °C in a humidified atmosphere with 5% CO_2. Confluent macrophages were treated with BSA or palmitate solutions (500 μM final concentration conjugated palmitate/BSA) for different time periods. For analysis of nitrite accumulation, the Griess method was used. Briefly, nitrites turn into a pink compound in contact with an acid solution (1% sulphanilamide and 0.1% N-(1-naphthyl) ethylenediamine (NEDA), and can be quantified by a colorimetric method at 540 nm in a microplate reader (Versamax Tunable Microplate reader, Molecular Devices, Sunnyvaley, CA, USA).

2.11. Oval cell culture and procedures

Wild-type and PTP1B-deficient mice were treated with 3,5-diethoxycarbonil-1,4-dihydrocollidine (DDC) diet for 14 days. Oval cell-enriched non-parenchymal cell fraction was isolated from these mice. Subsequently, oval cells were selected and expanded until generation of stable oval cell lines as described [34]. Cells were maintained in culture medium containing Williams E medium supplemented with 10% FBS, 2 mM L-glutamine, 20 mM Hepes, pH 7.5, 1 mM Na pyruvate, 17.6 mM $NaHCO_3$, 14 mM glucose, 100 nM Dexamethasone, 1 g/L insulin-transferrin-selenium, 10 ng/ml epidermal growth factor (EGF), and 10 ng/ml hepatocyte growth factor (HGF). For signaling experiments, cells were serum starved for 16 h prior to stimulation with HGF (40 ng/ml; Preprotech, London, UK). For immunofluorescence, cells were grown in polymer coverslip open microslides (Ibidi, ibidi GmbH, German) until 80% confluence was reached. Then, cells were washed twice with PBS, after that were fixed in 4% paraformaldehyde for 20 min at RT and then permeabilized with 0.1% Triton X-100 during 2 min. After that, cells were blocked in PBS-3% BSA during 2 h at room temperature. Primary antibodies (A6 kindly supplied by V. Factor (NIH, MD, USA)) or albumin (Merck Millipore) were applied for 1 h at 37 °C in PBS-1% BSA followed by 4×5 min washes in PBS, a 45 min incubation with fluorescence-conjugated secondary antibody (Alexa Fluor 565 goat anti-rat or Alexa Fluor 488 goat anti-rabbit, ThermoFisher Scientific) and four final washes of 5 min each in PBS. Immunofluorescence was examined in a confocal microscope LSM710 (Zeiss, Barcelona, Spain). Immunofluorescence mounting medium was from Vector (Burlingame, CA, USA). For 4,6-diamidino-2-phenylindole (DAPI) staining, cells were washed with PBS, fixed in methanol (−20 °C) for 2 min and stained with 1 μM DAPI for 5 min in the dark. After washing with PBS, nuclear morphology was analyzed by fluorescence or confocal microscopy. For evaluation of the proliferative capacity of oval cells, 150,000 cells were seeded in 6-well multiwell plates and maintained in complete culture medium up to 48 h. The proliferative capacity was analyzed at different time-periods by crystal violet staining.

2.12. Western blot analysis

After SDS-PAGE, gels were transferred to PVDF membranes and were blocked using 5% non-fat dried milk or 3% bovine serum albumin (BSA) in 10 mM Tris—HCl, 150 mM NaCl pH 7.5, and incubated overnight at 4 °C with several antibodies as indicated in 0.05% Tween-20, 10 mM Tris—HCl, 150 mM NaCl pH 7.5. Immunoreactive bands were visualized using the ECL western blotting protocol (Bio-Rad, Madrid, Spain). Densitometric analysis of the bands was performed using Image J software. Antibodies used were: anti-phospho Met (Tyr1234/1235) (#3126), anti-phospho ERK1/2 (Thr202/Tyr204) (#4370), and anti-ERK (#9102) from Cell Signaling Technology (Danvers, MA, USA), anti-PTP1B (07-088) from Merck Millipore, and anti-Met (sc-162) from Santa Cruz Biotechnology (Palo Alto, CA, USA).

2.13. Statistical analysis

Data are presented as mean ± SEM. Normal distribution was assessed by two different tests, Shapiro—Wilk and Kolmogorov—Smirnov tests. Data were compared by using one-way ANOVA or Kruskal—Wallis followed by a Bonferroni or Dunns test, respectively. The P values presented in figures and tables corresponded to post hoc test. All statistical analyses were performed using the GraphPad Prism 5.0 software (GraphPad Software Inc., San Diego, CA, USA) and SPSS 15.0 software (SPSS, Inc., Chicago, IL, USA). Differences were considered statistically significant at $P < 0.05$.

3. RESULTS

3.1. PTP1B deficiency accelerated MCD-induced NASH

To clarify the role of PTP1B in NASH, we analyzed wild-type (PTP1BWT) and PTP1B-deficient mice (PTP1BKO) fed chow diet (CHD) or methionine/choline-deficient diet (MCD) for 4 or 8 weeks. All mice lost about 25% of their initial body weight after 4 weeks on MCD or about 35% at 8 weeks regardless of the genotype (Supplementary Figure 1). As compared to animals fed CHD, mice receiving MCD displayed a significant loss in liver mass and in all pads of white adipose tissue (WAT) analyzed.

PTP1BWT mice fed MCD exhibited severe NASH features including steatosis, inflammation, and ballooning, and these effects were exacerbated at 8 weeks (Figure 1A). As expected, alanine aminotransferase (ALT) activity was significantly elevated compared to values of mice fed CHD. Moreover, *Fgf21* mRNA levels, a marker of liver damage in NASH [35], increased in a time-dependent manner (Figure 1B). Interestingly, PTP1B deficiency accelerated MCD-induced NASH as reflected by changes in liver histology, serum ALT, and *Fgf21* mRNA levels.

Serum TG levels decreased after MCD challenge due to the diet-induced impairment of hepatic export of VLDL, as previously described [24], being this reduction more pronounced in mice lacking PTP1B (Figure 1C). Although the MCD diet increased fat content in the liver of both genotypes, PTP1BKO mice gained hepatic TG in a faster manner compared with PTP1BWT animals (Figure 1D). In parallel to lipid accumulation, an enhanced increase of *Cd36* mRNA was observed in livers from PTP1BKO mice during the MCD challenge. Curiously, basal mRNA levels of this fatty acid transporter were lower in PTP1BKO mice (Figure 1D). Thus, we investigated the fatty acid uptake capacity and intracellular lipid accumulation under basal conditions in immortalized hepatocytes from both genotypes. The analysis of bromopalmitate uptake and Nile Red staining showed that PTP1B deficiency also reduced basal fatty acid transport and intracellular lipid content in hepatocytes (Figure 1E).

3.2. During the MCD challenge, infiltration of proinflammatory non-parenchymal cells (NPCs) was observed in livers from PTP1BWT mice and this effect was enhanced in PTP1BKO mice

Besides liver damage caused by fat deposition, NASH is characterized by focal inflammation. Hepatic mRNA levels of proinflammatory markers such us *Il1b*, *Il6*, and *Ccl2* were expressed at higher levels in livers from PTP1BKO mice after feeding MCD diet (Figure 2A). Interestingly, mRNA levels of M2 markers (*Il4*, *Il13*, and *Arg1*) were also augmented in the livers of those mice compared to PTP1BWT controls (Figure 2A).

Next, we evaluated the impact of PTP1B deficiency in the immune responses of the liver during NASH by isolating the NPCs populations followed by flow cytometry analysis in mice fed MCD for 4 and 8 weeks. Activated Kupffer cells ($Cd45^+Cd11b^+F4/80^+$) were similarly increased in both genotypes of mice after 4 weeks of MCD challenge, but, at 8 weeks, this population was significantly higher in PTP1BKO mice (Figure 2B). A similar pattern was found in recruited monocytes ($CD11b^+Ccr2^+$), particularly in the newly recruited monocyte subpopulation ($CD11b^+Ccr2^+Ly6C^+$) (Figure 2C). As reported by Zhang and co-workers [36], neutrophils play a key role in the establishment of NASH. Taking this into account, the analysis of the $Cd45^+Ly6G^+F480^-$ population showed a strong increase in livers from MCD-fed PTP1BKO mice at 4 and 8 weeks in comparison with the moderate increase of the PTP1BWT controls (Figure 3A). As reported in mice fed MCD for 4 weeks [37], the natural killer T (NKT) population ($Cd45^+Cd3^+NK1.1^+$) was depleted in both genotypes (Figure 3B), although depletion was higher in PTP1BWT livers. This depletion of the NKT population was maintained in PTP1BWT livers at 8 weeks of the MCD challenge, whereas in PTP1BKO livers the percentage of this population was further decreased compared to the levels found at 4 weeks. Interestingly, cytotoxic NKT cells ($Cd45^+Cd3^+Cd8^+NK1.1^+$) were elevated in PTP1BKO livers under basal conditions (CHD) and strongly increased after 8 weeks of MCD intervention in contrast with the moderate increase found in PTP1BWT livers (Figure 3C).

3.3. PTP1B deficiency enhanced the proinflammatory response in macrophages loaded with palmitate

In order to determine the impact of the macrophage population in the exacerbated proinflammatory response observed in the livers of PTP1BKO mice challenged with MCD diet, peritoneal macrophages were isolated from PTP1BWT and PTP1BKO mice and activated with palmitate as a proinflammatory stimulus, and the expression of a series of representative genes of the M1 response was determined. Figure 4A shows that palmitate-induced nitrite accumulation in macrophages lacking PTP1B was 2-fold higher than the effect found in macrophages from PTP1BWT mice in parallel to a significant up-regulation of *Nos2* expression (Figure 4B). Moreover, palmitate-mediated induction of *Il6*, *Il1b*, *Tnfa* and *Ccl2* mRNA levels was also enhanced in absence of PTP1B (Figure 4C).

3.4. PTP1B deficiency accelerates the reversion of NASH in a recovery dietary model

In order to determine whether PTP1B could also affect the reversion of MCD-induced NASH, we performed a recovery experimental model by switching mice already fed MCD to a CHD. For that goal, mice were re-fed with CHD after 8 weeks on MCD and the parameters studied above (Figure 1) were analyzed at 2, 4, and 7 days after the dietary change. Switching to CHD after 8 weeks of MCD diet resulted in a recovery of body weight, reaching the initial levels after one week (Supplementary Figure 2). Moreover, under these conditions restoration of all WAT pads

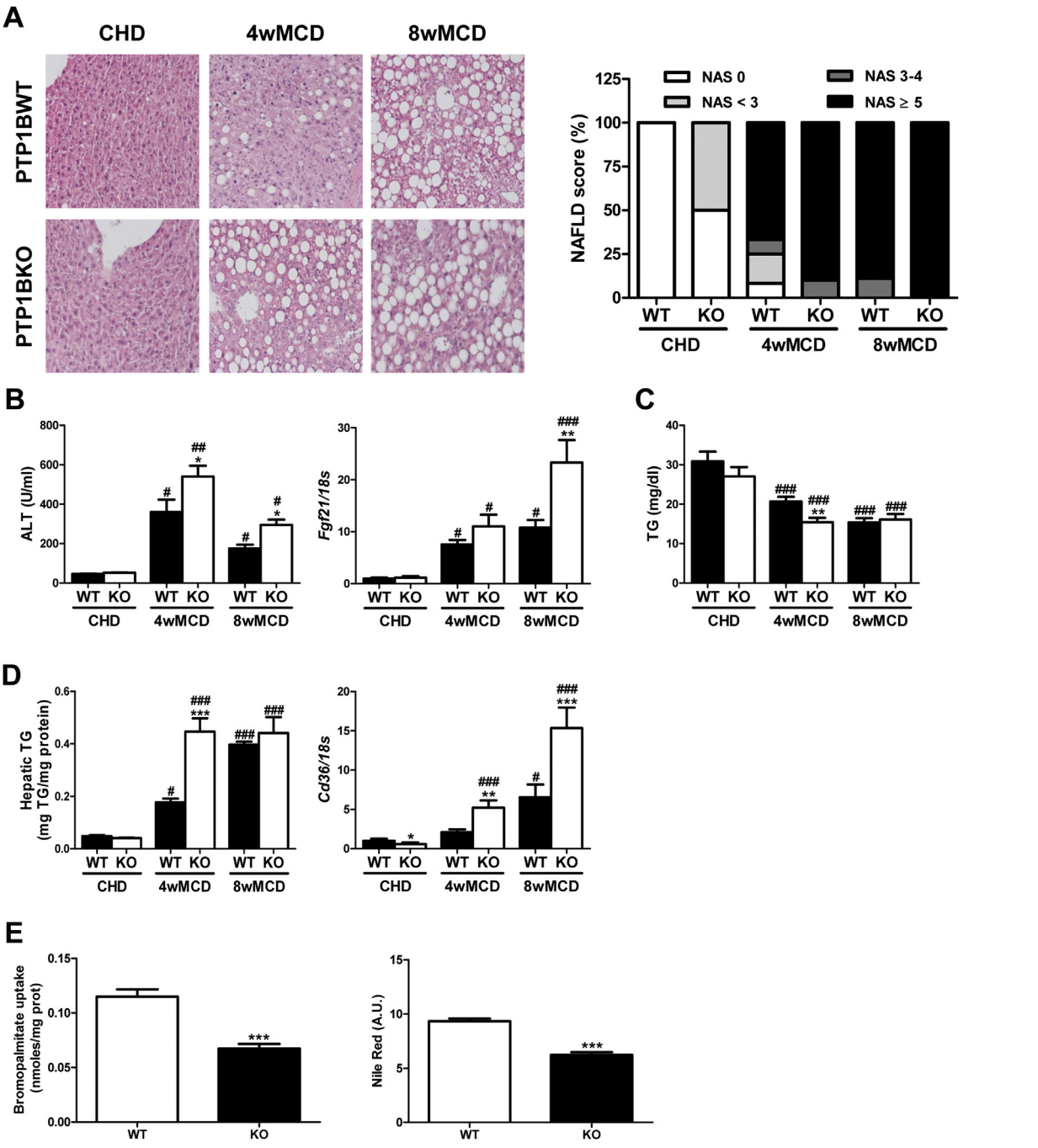

Figure 1: Lack of PTP1B accelerated MCD-induced NASH. A. Representative images of Hematoxylin & Eosin staining, and NAFLD score (NAS). **B.** Serum ALT and hepatic *Fgf21* mRNA levels. **C**. Serum TG levels. **D**. Hepatic TG content and *Cd36* mRNA levels. Experimental groups: PTP1BWT and PTP1BKO mice fed chow (CHD) or methionine/choline-deficient diet for 4 (4wMCD) or 8 weeks (8wMCD) (n = 8–12 animals/group). *P < 0.05, **P < 0.01 and ***P < 0.005, PTP1BKO vs. PTP1BWT; #P < 0.05, ##P < 0.01 and ###P < 0.005, 4wMCD or 8wMCD vs. CHD. **E**. Bromopalmitate uptake and Nile Red staining in PTP1BWT and PTP1BKO hepatocytes. (n = 4 independent experiments performed in duplicate). ***P < 0.005, KO vs. WT.

was observed and this effect was faster in PTP1BKO mice, particularly in the epididymal WAT depot.

NASH parameters such as NAFLD score, serum ALT, intrahepatic TG content, and *Fgf2*1 mRNA levels were normalized after the switch to CHD in both genotypes of mice, but this effect was accelerated in PTP1BKO mice compared with PTP1BWT controls (Figure 5A, B and D). Moreover, PTP1B deficiency improved the restoration of serum TG levels as early as 2 days after the recovery (Figure 5C). During the recovery period, *Cd36* mRNA significantly decreased in the livers of both genotypes (Figure 5D). Regarding inflammatory markers, mRNA levels of *Il1b*, *Il6*, and *Ccl2* decreased in both genotypes, although PTP1B deficiency accelerated this process (Figure 5E). Interestingly, the induction of the M2 markers by MCD observed in livers from PTP1BKO mice was suppressed after switching to CHD (Figure 5E).

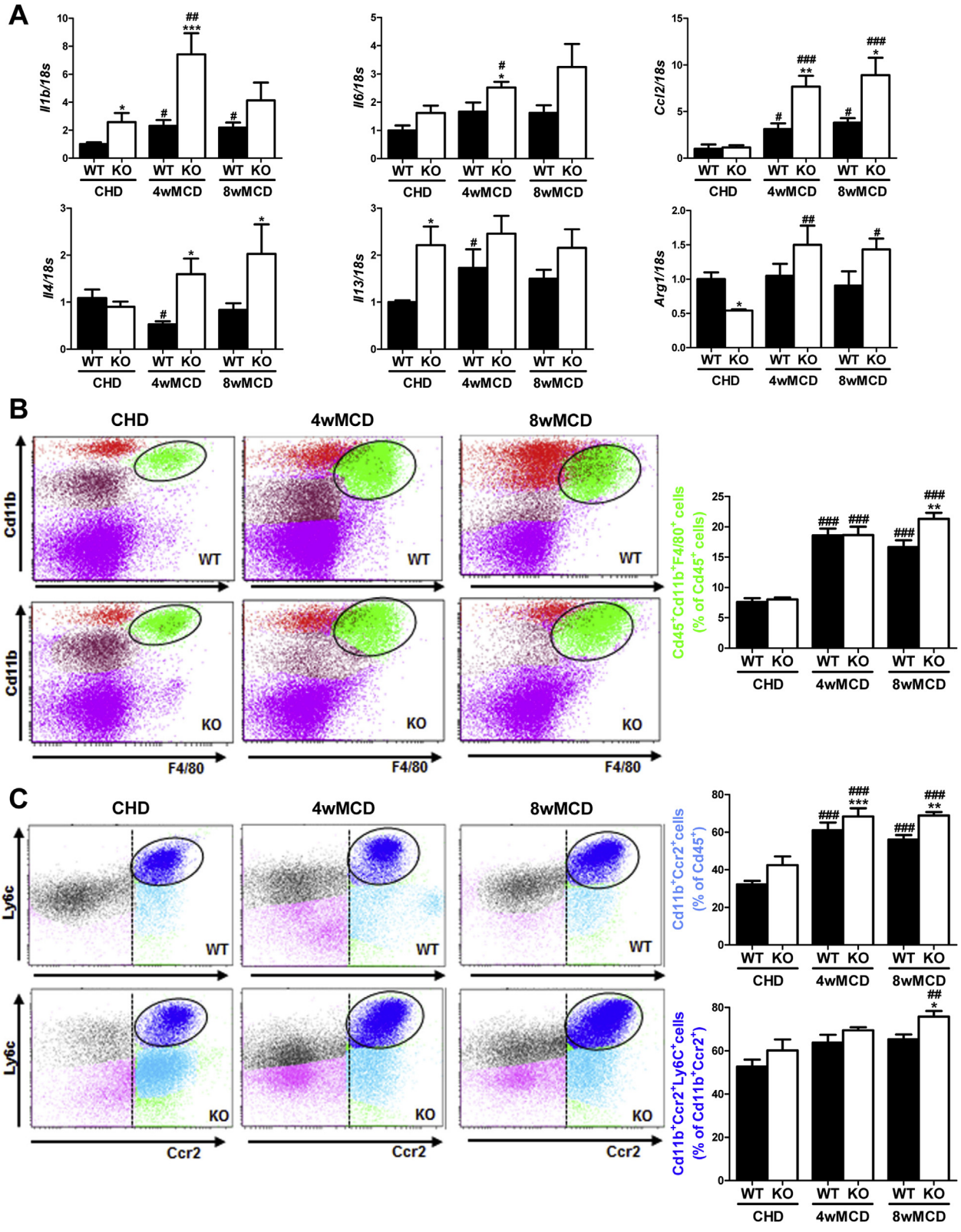

Figure 2: PTP1B deficiency enhanced an inflammatory response during the MCD diet challenge. A. Hepatic mRNA levels of inflammatory markers. **B, C**. Analysis of immune NPCs populations. Experimental groups: PTP1BWT and PTP1BKO mice fed chow (CHD) or methionine/choline-deficient diet for 4 (4wMCD) or 8 weeks (8wMCD) (n = 8–12 animals/group). *P < 0.05, **P < 0.01 and ***P < 0.001, PTP1BKO vs. PTP1BWT; #P < 0.05, ##P < 0.01 and ###P < 0.005, 4wMCD or 8wMCD vs. CHD.

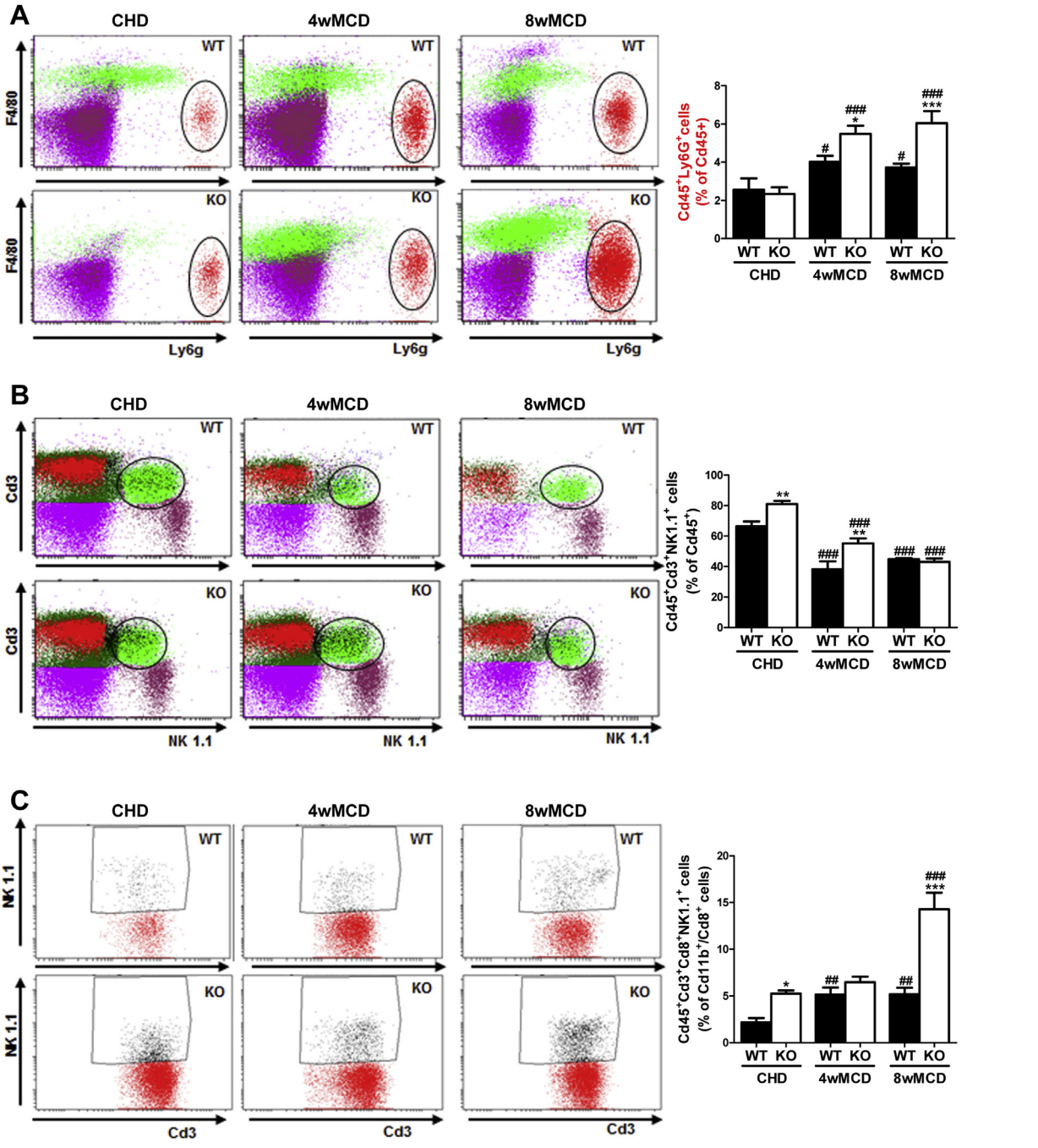

Figure 3: Differential effects on neutrophils and natural killer cells during the MCD challenge between genotypes. A, B, C. Analysis of immune NPCs populations. Experimental groups: PTP1BWT and PTP1BKO mice fed chow (CHD) or methionine/choline-deficient diet for 4 (4wMCD) or 8 weeks (8wMCD) (n = 8–12 animals/group). *P < 0.05, **P < 0.01 and ***P < 0.005, PTP1BKO vs. PTP1BWT; #P < 0.05, ##P < 0.01 and ###P < 0.005, 4wMCD or 8wMCD vs. CHD.

3.5. Analysis of NPCs populations during the recovery phase in livers from PTP1BWT and PTP1BKO mice

We next addressed the profile of the inflammatory NPCs populations during the recovery period. NPCs were isolated from mice fed MCD during 8 weeks and switched to CHD for 4 days. Recruited monocytes ($Cd11b^+Ccr2^+$) did not change in PTP1BWT livers during the recovery; however, in PTP1BKO mice, this population decreased significantly (Figure 6A). Interestingly, the newly recruited monocyte subpopulation ($Cd11b^+Ccr2^+Ly6C^+$) was increased in both genotypes (Figure 6A). Substantial differences among genotypes in the recovery phase were found in NKT cells ($Cd45^+Cd3^+NK1.1^+$) that decreased exclusively in PTP1BKO livers (Figure 6B). The decrease in NKT cells was particularly relevant in the cytotoxic NKT subpopulation ($Cd45^+Cd3^+Cd8^+NK1.1^+$) that was highly elevated in PTP1BKO mice after 8 weeks of MCD challenge and dramatically decreased at 4 days of the recovery, reaching similar levels found in PTP1BWT mice (Figure 6C).

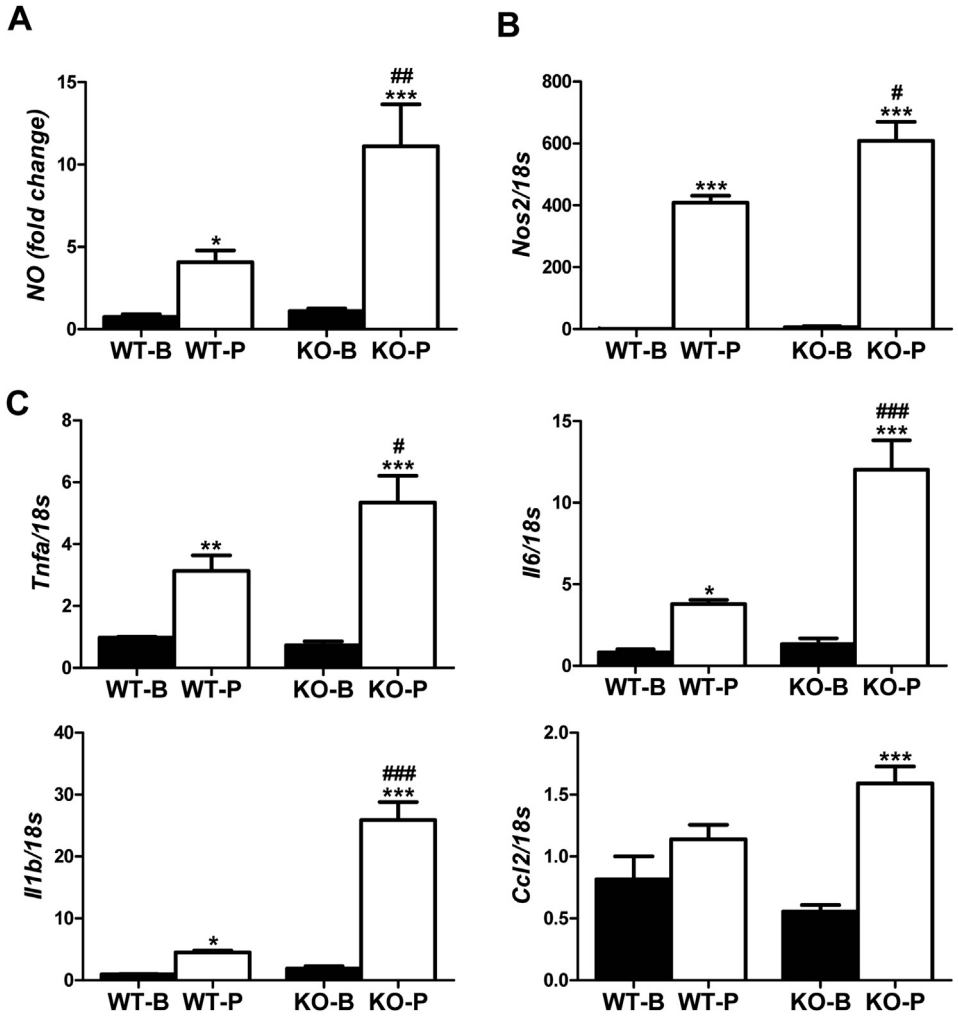

Figure 4: PTP1B deficiency increased the proinflammatory response in macrophages treated with palmitate. A. Nitrites accumulation. **B, C.** mRNA levels of inflammatory cytokines markers. Peritoneal macrophages were isolated from wild-type and PTP1B-deficient mice treated with palmitate 500 μM. (n = 3 independent experiments performed in triplicate). *P < 0.05, **P < 0.01 and ***P < 0.005, P vs. B; #P < 0.05, ##P < 0.01 and ###P < 0.005, KO vs. WT.

3.6. Enhanced proliferative capacity in livers from PTP1BKO mice

To investigate the possibility of a compensatory proliferative response of liver cells to MCD-induced NASH, Ki67 immunostaining was performed. The number of cells immunopositive for Ki67 was modestly increased in mice fed MCD for 8 weeks compared to mice fed CHD, although a higher elevation in livers from PTP1BKO mice was detected (Figure 7A and B). By contrast, the number of Ki67-positive cells markedly increased at 2–4 days of the recovery period, again with a more pronounced effect in PTP1BKO livers, suggesting a higher proliferative capacity of these liver cell population. Ki67 immunostaining declined after 7 days of the recovery (Figure 7A and B).

3.7. Markers of hepatic oval cells are increased in PTP1BKO mice with NASH and in livers from NASH patients

It is well known that, upon a severe liver injury, rodent oval cells are able to actively proliferate and to differentiate to mature hepatocytes. Based on that, we next evaluated the mRNA levels of two well-characterized oval cell markers cytokeratin 19 (*Krt19*) and EpCAM (*Epcam*) [38]. As shown in Figure 7C, *Epcam* mRNA was induced in the livers of mice fed MCD; this effect being significantly increased in PTP1BKO mice. After switching to CHD, *Epcam* mRNA decreased in the same way in both genotypes of mice. Regarding *Krt19* mRNA, it was increased by MCD intervention exclusively in the livers of PTP1BKO mice. In the recovery period, it was elevated in both genotypes after 4 days of the MCD withdrawal but, again, significant higher levels were detected in PTP1BKO mice. As occurred with *Epcam*, *Krt19* mRNA levels declined at day 7 of the recovery period in both genotypes of mice. Interestingly, in NASH patients (Supplementary Table 1), hepatic mRNA levels of *Epcam* and *Krt19* were up-regulated compared to individuals with normal liver (Figure 7D).

3.8. PTP1B deficiency enhances the induction of oval cell proliferation in the DDC model

In order to further decipher whether PTP1B is a key player in the plasticity of oval cells, we used a well-known and very efficient rodent model of liver damage associated to oval cells proliferation, the 3,5-diethoxycarbonil-1,4-dihydrocollidine (DDC)-supplemented diet [34]. Following feeding a DDC diet for 14 days, hepatocellular hypertrophy in centrilobular and periportal areas, known as ductular reaction, was detected. This was accompanied by the proliferation of biliary epithelial/oval cells in these areas achieved by cytokeratin 19 (CK19) immunostaining in liver sections from both genotypes

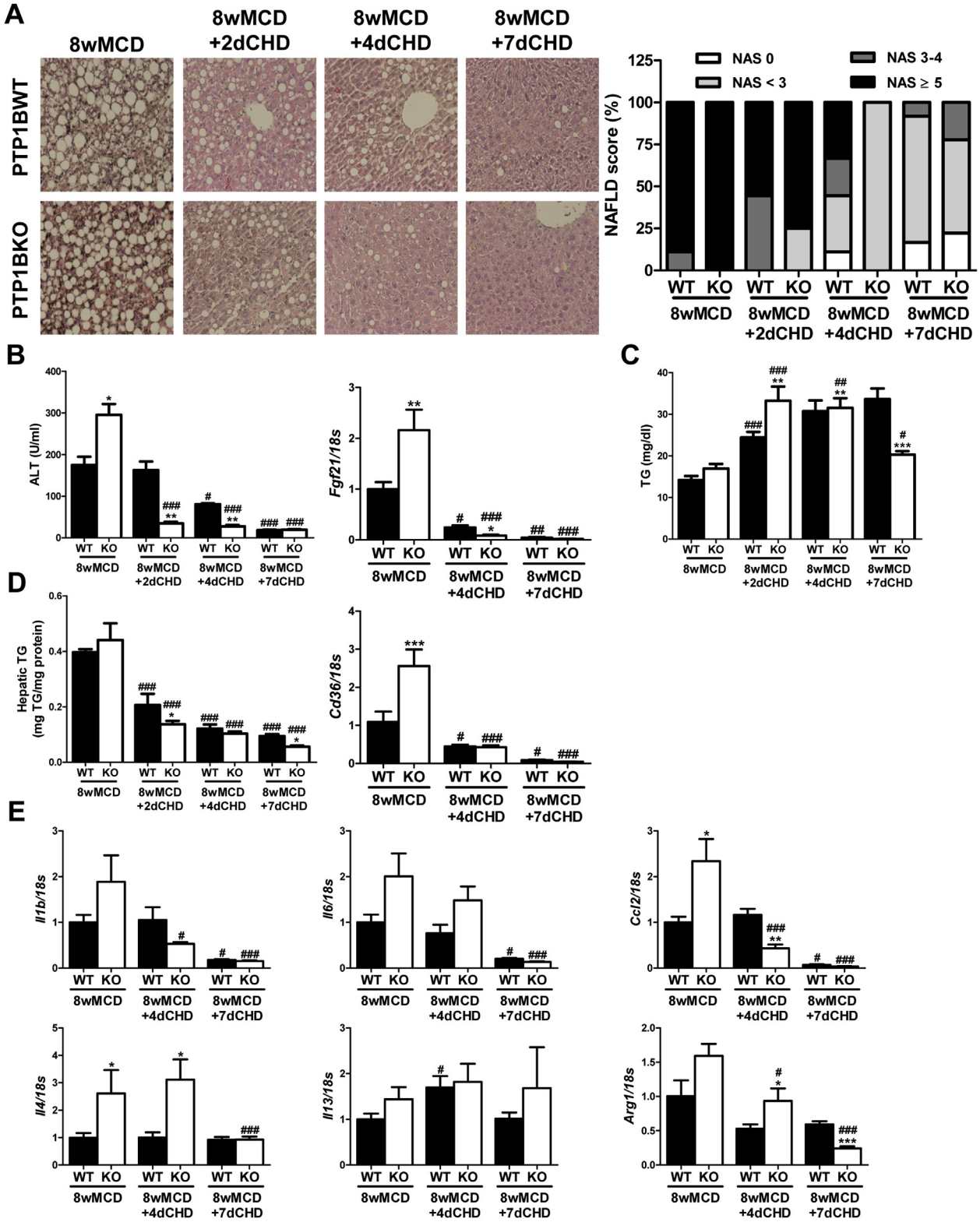

Figure 5: Histological and molecular characterization of livers from wild-type and PTP1B-deficient mice re-fed chow diet (CHD) after 8 weeks of methionine/choline-deficient diet (MCD). A. Representative images of Hematoxylin & Eosin staining, and NAFLD score (NAS). **B.** Serum ALT and hepatic *Fgf21* mRNA levels. **C.** Serum TG levels. **D.** Hepatic TG content and *Cd36* mRNA levels. **E.** Hepatic mRNA levels of inflammatory markers. Experimental groups: PTP1BWT and PTP1BKO re-fed chow diet for 2 (8wMCD+2dCHD), 4 (8wMCD+4dCHD) or 7 days (8wMCD+7dCHD) after 8 weeks of methionine/choline-deficient diet (8wMCD). (n = 8–12 animals/group) *P < 0.05, **P < 0.01 and ***P < 0.005, PTP1BKO vs. PTP1BWT; #P < 0.05, ##P < 0.01 and ###P < 0.005, 8wMCD+CHD vs. 8wMCD.

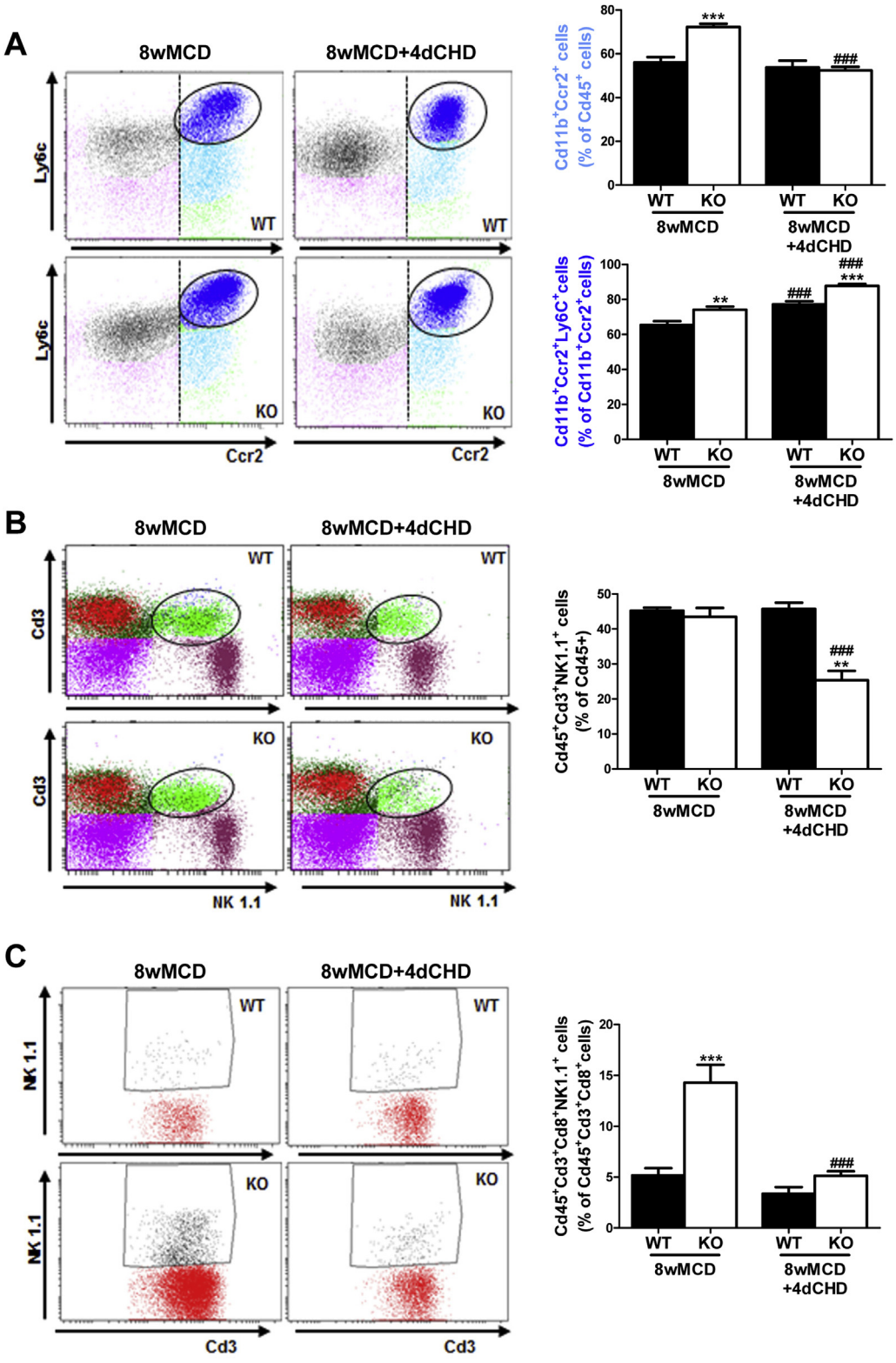

Figure 6: Analysis of NPCs population during the recovery phase in livers from PTP1BWT and PTP1BKO mice. A, B, C. Analysis of immune NPCs populations. Experimental groups: PTP1BWT and PTP1BKO re-fed chow diet for 4 (8wMCD+4dCHD) after 8 weeks of methionine/choline-deficient diet (8wMCD). (n = 8–12 animals/group) **P < 0.01 and ***P < 0.005, PTP1BKO vs. PTP1BWT; ###P < 0.005, 8wMCD+4dCHD vs. 8wMCD.

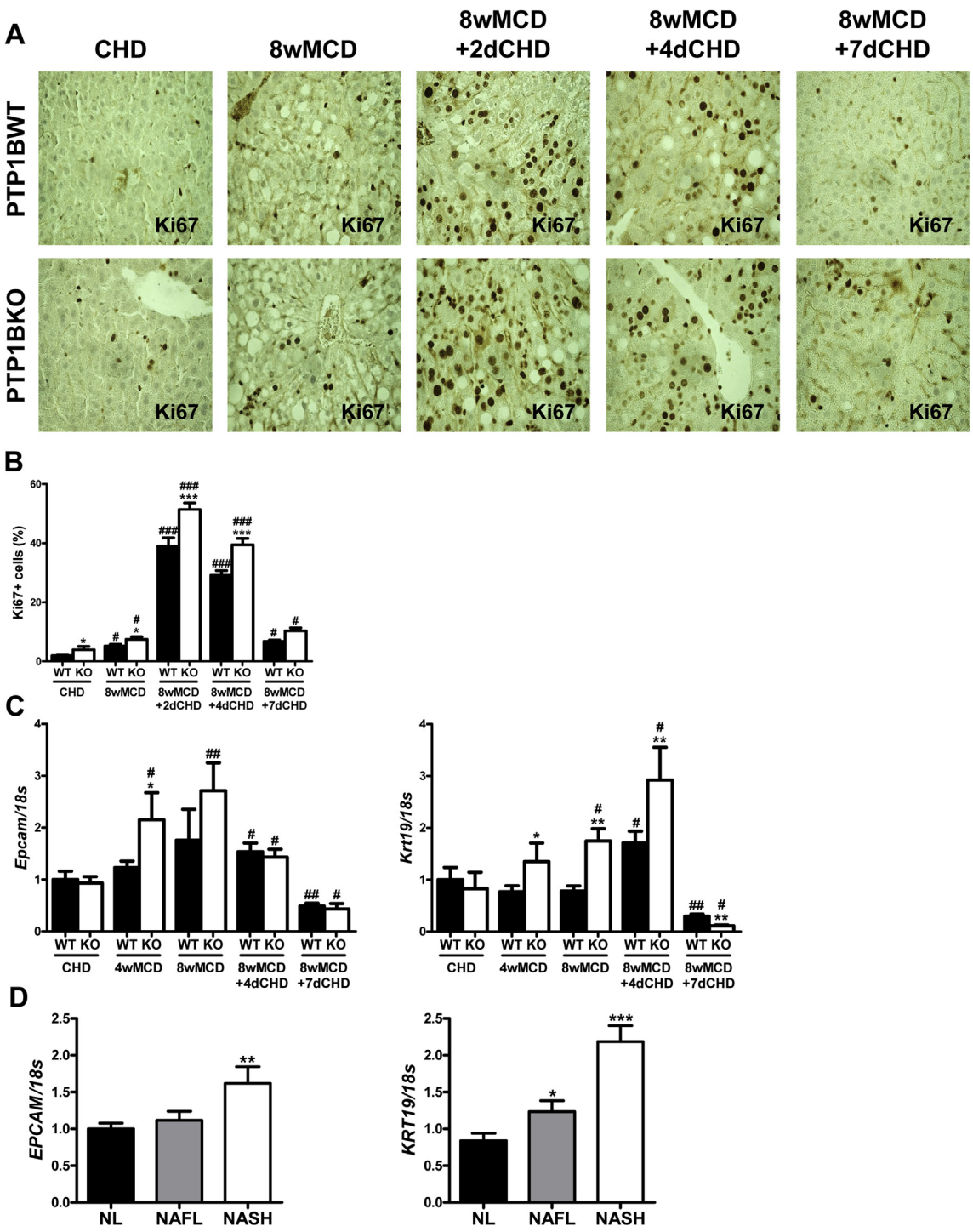

Figure 7: Enhanced proliferative capacity and expression of oval cell markers in livers from PTP1BKO mice. A. Representative images of Ki67 immunostaining. **B.** Quantification of Ki67-positive cells. **C.** Hepatic mRNA levels of oval cell markers. Experimental groups: PTP1BWT and PTP1BKO fed chow (CHD) or methionine/choline-deficient diet for 4 (4wMCD) or 8 weeks (8wMCD), or re-fed chow diet for 2 (8wMCD+2dCHD), 4 (8wMCD+4dCHD) or 7 days (8wMCD+7dCHD) after 8 weeks of MCD. (n = 8–12 animals/group) *P < 0.05, **P < 0.01 and ***P < 0.005, PTP1BKO vs. PTP1BWT; #P < 0.05, ##P < 0.01 and ###P < 0.005, 8wMCD+CHD vs. 8wMCD. **D.** Hepatic mRNA levels of oval cell markers in livers from NAFL and NASH patients. *P < 0.05, **P < 0.01 and ***P < 0.005, NAFL or NASH vs. NL.

(Figure 8A). We also found increased intensity and expanded areas of CK19 immunostaining in livers lacking PTP1B. Consistent with this, PTP1B-deficient mice treated with DDC diet presented higher levels of *Krt19* and *Epcam* mRNA levels in the liver than PTP1BWT mice (Figure 8B).

To get new insights on the impact of PTP1B deficiency in oval cells, we isolated oval cells from DDC-treated PTP1BWT and PTP1BKO livers and established them in culture. We characterized oval cell markers by immunostaining with anti-albumin and anti-A6 antibodies. As shown in Figure 8C, both genotypes of oval cells were positive for

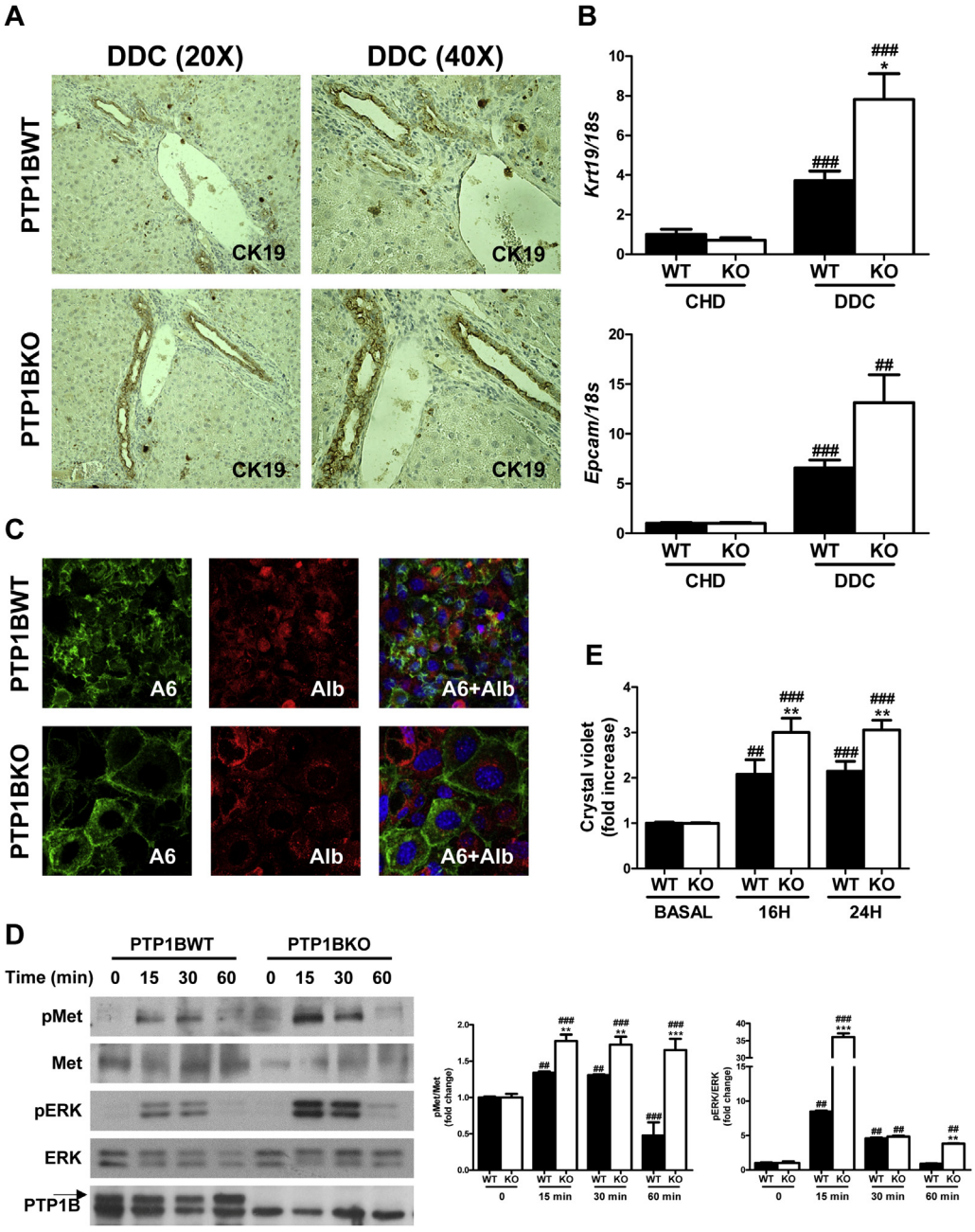

Figure 8: Characterization and responsiveness to HGF of oval cell isolated from wild-type and PTP1B-deficient mice treated with DDC. A. Representative images of cytokeratin 19 (CK19) immunostaining. **B.** Hepatic mRNA levels of oval cell markers. Experimental groups: PTP1BWT and PTP1BKO treated with DDC for 14 days. ($n = 6-8$ animals/group) *P $<$ 0.05, PTP1BKO vs. PTP1BWT; ##P $<$ 0.01 and ###P $<$ 0.005, DDC vs. CHD. **C.** Representative images of immunofluorescence of oval cells markers. **D.** Representative blots with the indicated antibodies and quantification of blots corresponding to all experiments performed. **E.** Crystal violet assay. PTP1BWT and PTP1BKO oval cells were isolated from wild-type and PTP1B-deficient mice treated with DDC ($n = 3$ independent experiments performed in triplicate). **P $<$ 0.01 and ***P $<$ 0.005, KO vs. WT; ##P $<$ 0.01 and ###P $<$ 0.005, vs. basal condition.

albumin and A6. Given that HGF is a well-known mitogen for liver oval cells [34,39], we checked that oval cell lines expressed the HGF receptor (Met) and responded to HGF stimulation by inducing its tyrosine phosphorylation. As shown in Figure 8D, oval cells stimulated with HGF (40 ng/ml) induced the tyrosine phosphorylation of the HGF receptor (Met) in a time-dependent manner. Interestingly, Met phosphorylation was enhanced in PTP1BKO oval cells, suggesting that these cells are hypersensitive to HGF stimulation in a similar way as hepatocytes [10]. Activation of downstream targets of Met, such as extracellular signal–regulated kinase 1/2 (ERK1/2), was also enhanced when PTP1B was deleted. Of note, the lack of PTP1B in oval cells was verified by western blot. Finally, we analyzed the proliferation capacity of both genotypes of cells in response to complete medium containing HGF. Figure 8E shows that PTP1B deficiency in oval cells enhanced their proliferation capacity compared with the wild-type controls.

4. DISCUSSION

The role of PTP1B as a metabolic modulator has been extensively reported in preclinical models of diet-induced insulin resistance and obesity in mice with global or tissue-specific deletion of the *Ptpn1* gene [4,6] as well as in humans [40]. On the other hand, NAFLD is a chronic liver disease that, in its initial stages, is directly associated with fatty liver and hepatic insulin resistance, in which PTP1B plays also a major role [6,27,41]. Despite this extensive knowledge, much less is known on the involvement of PTP1B during NAFLD progression, particularly in NASH, in which the inflammatory component is crucial for disease progression. This is a particular relevant issue because a dual role of PTP1B has been described; in non-immune cells such as hepatocytes promoting insulin resistance and cell death [5,9] and in immune cells (macrophages and B cells) inhibiting the proinflammatory responses [11–13,42]. Importantly, as PTP1B-deficient mice do not develop hepatic steatosis on a HFD [10] or during aging [27], experimental conditions that implicate obesity/adiposity, to unravel a possible dual role of this phosphatase in NASH, we made use of the MCD diet as a non-obese trigger of NASH that concurs mainly with steatosis and inflammation, two effects oppositely modulated by PTP1B.

MCD diet induced NASH in a time dependent-manner in both PTP1BWT and PTP1BKO mice as demonstrated by the histopathological evaluation of liver sections, elevations of serum ALT and hepatic *Fgf21* mRNA, which are indicative of liver injury [43], and by increases in *Cd36* mRNA expression and intrahepatic TG content, an indicator of enhanced lipid overload. Importantly, our results have revealed that all these effects were accelerated in PTP1BKO mice, suggesting that PTP1B deficiency increases the susceptibility to lipid accumulation and, consequently, accelerates and sustains the lipotoxic damage in the liver. Curiously, basal *Cd36* mRNA levels in the liver as well as fatty acid uptake in hepatocytes were lower in the absence of PTP1B. Therefore, further investigation is needed to identify a possible role of PTP1B in fatty acid transport.

As stated above, MCD challenge induced hepatic focal inflammation that is likely due to hepatocyte lipotoxicity [44]. In agreement with Nasimian and co-workers [45], and with the increased steatosis found in MCD-fed PTP1BKO mice compared to the PTP1BWT controls, the lack of PTP1B resulted in a higher expression of the M1 responsive genes in macrophages loaded with palmitate. Likewise, mRNA levels of M1 proinflammatory cytokines were strongly elevated in PTP1BKO livers from MCD-fed mice. In this context, flow cytometry analysis revealed higher presence of resident macrophages (Kupffer cells) in PTP1BKO livers after 8 weeks of MCD intervention. Interestingly, M2 markers, particularly IL4 and arginase 1, were also induced in livers from PTP1BKO during the time-course of MCD dietary intervention, reaching higher levels than those of the PTP1BWT controls. These results suggest that in PTP1BKO livers, the M2 response might be a compensatory mechanism against an excessive M1-mediated inflammation. A more extensive analysis of the NPCs in the liver identified higher recruitment of monocytes in PTP1BKO mice under MCD at both 4 and 8 weeks. Notably, the percentage of newly recruited monocytes ($Cd11b^{+}Ccr2^{+}Ly6C^{+}$) was only increased in mice lacking PTP1B at 8 weeks, likely due to the sustained lipotoxic damage as suggested by Xiao and co-workers [46]. Infiltration of neutrophils is a main immune feature of the early stage of NASH as demonstrated by Zhang and co-workers [36]. In this regard, the livers of both genotypes of mice responded with an early and sustained elevation of infiltrated neutrophils ($Cd45^{+}Ly6G^{+}$), although this response was manifested more elevated in PTP1BKO mice. Also, NKT ($Cd45^{+}Cd3^{+}NK1.1^{+}$) cells expansion is a hallmark of enhanced NASH in rodents and humans [47], and depletion of this population has been reported in mice fed MCD for 4 weeks [37] an effect abolished in immunized mice with more severe NASH. Our results in mice fed MCD for 4 weeks are totally in agreement with these data since PTP1BKO mice presented lower NKT cells depletion at this time-period in which substantial differences in the NAFLD score were detected in comparison with PTP1BWT mice. Another relevant piece of data was found in the cytotoxic NKT subpopulation ($Cd45^{+}Cd3^{+}Cd8^{+}NK1.1^{+}$), which presented a significant increase in PTP1BKO mice after 8 weeks of MCD challenge. In this regard, increases in both $Cd8^{+}$T and NKT cells have been recently described as an immune feature of NASH in HFHC obesogenic murine model (Bhattacharjee et al., *in press*). Altogether, our data strongly suggest that the differences in lipotoxicity between PTP1BKO and PTP1BWT livers parallel with the profile of recruitment of inflammatory cells populations.

After the establishment of NASH, we implemented a recovery experimental model by replacing MCD diet for CHD. This dietary switch almost reversed all NASH characteristics in both genotypes after 7 days in agreement with other studies performed in this intervention model [44,48]. Of relevance and opposite with its effects on NASH progression, the lack of PTP1B accelerated the reversion of NASH. In fact, a more profound drop of intrahepatic TG content and transaminase levels together with an elevation of serum TG were detected, particularly at a very early period (2 days) of the recovery phase. Interestingly, these changes are likely to be responsible of the recovery of the fat depots that was augmented in PTP1BKO mice. In addition, after 4 days of recovery, the time at which the differences in the NAFLD score between genotypes were more evident, *Ccl2 and Il1b* mRNA levels decreased significantly in PTP1BKO compared to the PTP1BWT livers concurrently with the maintenance of the expression of M2 markers. Indeed, a more detailed analysis of NPCs revealed decreases in recruited monocytes and cytotoxic NKT cells in PTP1BKO mice.

The acceleration of NASH reversion in PTP1BKO mice was not surprising since our previous work demonstrated that PTP1B deficiency improves liver regeneration in mice after partial hepatectomy [10] and protects against cell death [8], indicating a higher proliferative/survival capacity of liver cells in the absence of PTP1B. Indeed, we found a higher proliferative capacity of the livers from PTP1BKO mice particularly during the early phases of NASH reversion achieved by an increased number of Ki67-positive cells. The molecular mechanism responsible of this effect likely involve tyrosine kinase receptors such as EGF receptor, HGF receptor (Met) or insulin-like growth factor-1 receptor (IGF1R), implicated in the control of proliferation and survival of hepatocytes, all of them dephosphorylated and inactivated by PTP1B [49]. In this regard, we have described that PTP1B deficiency increases liver growth enhancing the STAT5B/IGF1/IGF1R axis during suckling [50]. In addition, the faster recovery of PTP1BKO livers against NASH damage might also involve an effect on hepatic oval cells since their proliferation positively correlates with the extent of liver damage [51]. The role of oval cells in chronic liver damage is a matter of intense debate nowadays, having been reported both proregenerative and profibrotic roles [52]. Our data showing a greater oval cell expansion in PTP1BKO livers that is coincident with a more efficient recovery from liver damage during NASH suggest that these cells could be actively contributing to the regression of the disease. We confirmed these results by treating both genotypes of mice with DDC, a specific dietary model of oval cell expansion, and found that the lack of PTP1B enhanced hepatic mRNA levels of the oval cells markers CK19 and EpCAM compared to the controls, and induced a

more evident CK19-immunoreactive ductular reaction. In the light of our data, a recent study has reported an enhanced hepatic regeneration in mice with fibrosis by transplantation of differentiated oval-like cells [53]. Although chronic loss of hepatocytes is associated with regenerative efforts characterized by continuous hepatocyte proliferation and often has adverse consequences such as development of cirrhosis or liver cancer [54,55], the marked decrease in Ki67 positive cells at the end of the recovery phase, where no evidences of liver damage were observed, provide evidence of a controlled proliferative response of the liver under our experimental model.

Our initial experiments performed in oval cells isolated from PTP1BKO livers revealed an enhanced response to HGF-mediated signaling and proliferation compared with oval cells isolated from PTP1BWT livers. These results are in agreement with the enhanced HGF signaling previously found in PTP1BKO hepatocytes after partial hepatectomy [10] or acute liver injury [9], and highlight a unique role of this phosphatase in modulating the regenerative responses of the liver against both acute [9,10] and chronic damage (this study). This relevant issue deserves future research since it might offer a new therapeutic option to combat NASH.

In conclusion, this study has provided for the first time an experimental model evidencing the duality of PTP1B actions in the liver. Our results strongly suggest that during NASH progression PTP1B restrains inflammation, whereas in NASH reversion, this phosphatase targets the proliferative responses mediated by Met signaling in oval liver cells. This duality of PTP1B actions must be recognized for pharmacological purposes in chronic liver diseases such as NASH.

ACKNOWLEDGEMENTS

This work was funded by SAF2015-65267-R (MINECO/FEDER), CIBERdem (ISCIII, Spain), INFLAMES (ISCIII PIE14/00045, co-funded by ERDF, "Investing in your future") to A.M.V; IJCI-2014-19381 (MINECO/FEDER) to P.R and A.M.V; CP14/00181 and PI16/00823 (ISCIII/FEDER) and CIBERehd (ISCIII, Spain) to A.G-R; BFU2015-65937-R (MINECO/FEDER), 67-2015 (Department of Health, Navarra Government) and CIBERobn (ISCIII, Spain) to M.J.M; SAF2015-69145-R (MINECO/FEDER) to A.S. A.A. was recipient of a Marie Curie ESR contract from IT-LIVER (Marie Curie Action of the FP7-2012, grant agreement 316549). We also acknowledge the European Union, project H2020-MSCA-ITN TREATMENT Grant Agreement number: 721236.

CONFLICT OF INTEREST

None declared.

APPENDIX A. SUPPLEMENTARY DATA

Supplementary data related to this article can be found at https://doi.org/10.1016/j.molmet.2017.10.008.

REFERENCES

[1] Seely, B.L., Staubs, P.A., Reichart, D.R., Berhanu, P., Milarski, K.L., Saltiel, A.R., et al., 1996. Protein tyrosine phosphatase 1B interacts with the activated insulin receptor. Diabetes 45:1379—1385.

[2] Zabolotny, J.M., Bence-Hanulec, K.K., Stricker-Krongrad, A., Haj, F., Wang, Y., Minokoshi, Y., et al., 2002. PTP1B regulates leptin signal transduction in vivo. Developmental Cell 2:489—495.

[3] Elchebly, M., Payette, P., Michaliszyn, E., Cromlish, W., Collins, S., Loy, A.L., et al., 1999. Increased insulin sensitivity and obesity resistance in mice lacking the protein tyrosine phosphatase-1B gene. Science 283: 1544—1548.

[4] Klaman, L.D., Boss, O., Peroni, O.D., Kim, J.K., Martino, J.L., Zabolotny, J.M., et al., 2000. Increased energy expenditure, decreased adiposity, and tissue-specific insulin sensitivity in protein-tyrosine phosphatase 1B-deficient mice. Molecular Cell Biology 20:5479—5489.

[5] Haj, F.G., Zabolotny, J.M., Kim, Y.B., Kahn, B.B., Neel, B.G., 2005. Liver-specific protein-tyrosine phosphatase 1B (PTP1B) re-expression alters glucose homeostasis of PTP1B-/-mice. Journal of Biological Chemistry 280: 15038—15046.

[6] Delibegovic, M., Zimmer, D., Kauffman, C., Rak, K., Hong, E.G., Cho, Y.R., et al., 2009. Liver-specific deletion of protein-tyrosine phosphatase 1B (PTP1B) improves metabolic syndrome and attenuates diet-induced endoplasmic reticulum stress. Diabetes 58:590—599.

[7] Owen, C., Lees, E.K., Grant, L., Zimmer, D.J., Mody, N., Bence, K.K., et al., 2013. Inducible liver-specific knockdown of protein tyrosine phosphatase 1B improves glucose and lipid homeostasis in adult mice. Diabetologia 56: 2286—2296.

[8] Gonzalez-Rodriguez, A., Escribano, O., Alba, J., Rondinone, C.M., Benito, M., Valverde, A.M., 2007. Levels of protein tyrosine phosphatase 1B determine susceptibility to apoptosis in serum-deprived hepatocytes. Journal of Cell Physiology 212:76—88.

[9] Sangwan, V., Paliouras, G.N., Cheng, A., Dube, N., Tremblay, M.L., Park, M., 2006. Protein-tyrosine phosphatase 1B deficiency protects against Fas-induced hepatic failure. Journal of Biological Chemistry 281:221—228.

[10] Revuelta-Cervantes, J., Mayoral, R., Miranda, S., Gonzalez-Rodriguez, A., Fernandez, M., Martin-Sanz, P., et al., 2011. Protein Tyrosine Phosphatase 1B (PTP1B) deficiency accelerates hepatic regeneration in mice. American Journal of Pathology 178:1591—1604.

[11] Aoki, N., Matsuda, T., 2000. A cytosolic protein-tyrosine phosphatase PTP1B specifically dephosphorylates and deactivates prolactin-activated STAT5a and STAT5b. Journal of Biological Chemistry 275:39718—39726.

[12] Lu, X., Malumbres, R., Shields, B., Jiang, X., Sarosiek, K.A., Natkunam, Y., et al., 2008. PTP1B is a negative regulator of interleukin 4-induced STAT6 signaling. Blood 112:4098—4108.

[13] Myers, M.P., Andersen, J.N., Cheng, A., Tremblay, M.L., Horvath, C.M., Parisien, J.P., et al., 2001. TYK2 and JAK2 are substrates of protein-tyrosine phosphatase 1B. Journal of Biological Chemistry 276:47771—47774.

[14] Than, N.N., Newsome, P.N., 2015. A concise review of non-alcoholic fatty liver disease. Atherosclerosis 239:192—202.

[15] Chalasani, N., Younossi, Z., Lavine, J.E., Diehl, A.M., Brunt, E.M., Cusi, K., et al., 2012. The diagnosis and management of non-alcoholic fatty liver disease: practice guideline by the American gastroenterological association, American association for the study of liver diseases, and American College of gastroenterology. Gastroenterology 142:1592—1609.

[16] Day, C.P., James, O.F., 1998. Steatohepatitis: a tale of two "hits"? Gastroenterology 114:842—845.

[17] Stankovic, M.N., Mladenovic, D.R., Duricic, I., Sobajic, S.S., Timic, J., Jorgacevic, B., et al., 2014. Time-dependent changes and association between liver free fatty acids, serum lipid profile and histological features in mice model of nonalcoholic fatty liver disease. Archives of Medical Research 45:116—124.

[18] Morinaga, H., Mayoral, R., Heinrichsdorff, J., Osborn, O., Franck, N., Hah, N., et al., 2015. Characterization of distinct subpopulations of hepatic macrophages in HFD/obese mice. Diabetes 64:1120—1130.

[19] Duncan, A.W., Dorrell, C., Grompe, M., 2009. Stem cells and liver regeneration. Gastroenterology 137:466—481.

[20] Fausto, N., 2004. Liver regeneration and repair: hepatocytes, progenitor cells, and stem cells. Hepatology 39:1477—1487.

[21] Farber, E., 1956. Similarities in the sequence of early histological changes induced in the liver of the rat by ethionine, 2-acetylamino-fluorene, and 3'-methyl-4-dimethylaminoazobenzene. Cancer Research 16:142—148.

[22] Gaudio, E., Carpino, G., Cardinale, V., Franchitto, A., Onori, P., Alvaro, D., 2009. New insights into liver stem cells. Digestive and Liver Disease 41: 455–462.
[23] Oz, H.S., Chen, T.S., Neuman, M., 2008. Methionine deficiency and hepatic injury in a dietary steatohepatitis model. Digestive Diseases and Sciences 53: 767–776.
[24] Rinella, M.E., Elias, M.S., Smolak, R.R., Fu, T., Borensztajn, J., Green, R.M., 2008. Mechanisms of hepatic steatosis in mice fed a lipogenic methionine choline-deficient diet. The Journal of Lipid Research 49:1068–1076.
[25] Leclercq, I.A., Farrell, G.C., Field, J., Bell, D.R., Gonzalez, F.J., Robertson, G.R., 2000. CYP2E1 and CYP4A as microsomal catalysts of lipid peroxides in murine nonalcoholic steatohepatitis. Journal of Clinical Investigation 105:1067–1075.
[26] Demir, M., Lang, S., Steffen, H.M., 2015. Nonalcoholic fatty liver disease – current status and future directions. Journal of Digestive Diseases 16: 541–557.
[27] Gonzalez-Rodriguez, A., Mas-Gutierrez, J.A., Mirasierra, M., Fernandez-Perez, A., Lee, Y.J., Ko, H.J., et al., 2012. Essential role of protein tyrosine phosphatase 1B in obesity-induced inflammation and peripheral insulin resistance during aging. Aging Cell 11:284–296.
[28] Kleiner, D.E., Brunt, E.M., Van Natta, M., Behling, C., Contos, M.J., Cummings, O.W., et al., 2005. Design and validation of a histological scoring system for nonalcoholic fatty liver disease. Hepatology 41:1313–1321.
[29] Brunt, E.M., Janney, C.G., Di Bisceglie, A.M., Neuschwander-Tetri, B.A., Bacon, B.R., 1999. Nonalcoholic steatohepatitis: a proposal for grading and staging the histological lesions. American Journal of Gastroenterology 94: 2467–2474.
[30] Bligh, E.G., Dyer, W.J., 1959. A rapid method of total lipid extraction and purification. Canadian Journal of Biochemistry and Physiology 37:911–917.
[31] Gonzalez-Rodriguez, A., Mayoral, R., Agra, N., Valdecantos, M.P., Pardo, V., Miquilena-Colina, M.E., et al., 2014. Impaired autophagic flux is associated with increased endoplasmic reticulum stress during the development of NAFLD. Cell Death & Disease 5:e1179.
[32] Sanz-Garcia, C., Ferrer-Mayorga, G., Gonzalez-Rodriguez, A., Valverde, A.M., Martin-Duce, A., Velasco-Martin, J.P., et al., 2013. Sterile inflammation in acetaminophen-induced liver injury is mediated by Cot/tpl2. Journal of Biological Chemistry 288:15342–15351.
[33] Traves, P.G., Pardo, V., Pimentel-Santillana, M., Gonzalez-Rodriguez, A., Mojena, M., Rico, D., et al., 2014. Pivotal role of protein tyrosine phosphatase 1B (PTP1B) in the macrophage response to pro-inflammatory and anti-inflammatory challenge. Cell Death & Disease 5:e1125.
[34] del Castillo, G., Factor, V.M., Fernandez, M., Alvarez-Barrientos, A., Fabregat, I., Thorgeirsson, S.S., et al., 2008. Deletion of the Met tyrosine kinase in liver progenitor oval cells increases sensitivity to apoptosis in vitro. American Journal of Pathology 172:1238–1247.
[35] Valdecantos, M.P., Pardo, V., Ruiz, L., Castro-Sanchez, L., Lanzon, B., Fernandez-Millan, E., et al., 2017. A novel glucagon-like peptide 1/glucagon receptor dual agonist improves steatohepatitis and liver regeneration in mice. Hepatology 65:950–968.
[36] Zang, S., Wang, L., Ma, X., Zhu, G., Zhuang, Z., Xun, Y., et al., 2015. Neutrophils play a crucial role in the early stage of nonalcoholic steatohepatitis via neutrophil elastase in mice. Cell Biochemistry and Biophysics 73:479–487.
[37] Sutti, S., Jindal, A., Locatelli, I., Vacchiano, M., Gigliotti, L., Bozzola, C., et al., 2014. Adaptive immune responses triggered by oxidative stress contribute to hepatic inflammation in NASH. Hepatology 59:886–897.
[38] Chen, J.Z., Hong, H., Xiang, J., Xue, L., Zhao, G.Q., 2003. A selective tropism of transfused oval cells for liver. World Journal of Gastroenterology 9:544–546.
[39] Suarez-Causado, A., Caballero-Diaz, D., Bertran, E., Roncero, C., Addante, A., Garcia-Alvaro, M., et al., 2015. HGF/c-Met signaling promotes liver progenitor cell migration and invasion by an epithelial-mesenchymal transition-independent, phosphatidyl inositol-3 kinase-dependent pathway in an in vitro model. Biochimica et Biophysica Acta 1853:2453–2463.
[40] Ahmad, F., Considine, R.V., Bauer, T.L., Ohannesian, J.P., Marco, C.C., Goldstein, B.J., 1997. Improved sensitivity to insulin in obese subjects following weight loss is accompanied by reduced protein-tyrosine phosphatases in adipose tissue. Metabolism 46:1140–1145.
[41] Zabolotny, J.M., Kim, Y.B., Welsh, L.A., Kershaw, E.E., Neel, B.G., Kahn, B.B., 2008. Protein-tyrosine phosphatase 1B expression is induced by inflammation in vivo. Journal of Biological Chemistry 283:14230–14241.
[42] Heinonen, K.M., Dube, N., Bourdeau, A., Lapp, W.S., Tremblay, M.L., 2006. Protein tyrosine phosphatase 1B negatively regulates macrophage development through CSF-1 signaling. Proceedings of the National Academy of Sciences of the United States of America 103:2776–2781.
[43] Fisher, F.M., Chui, P.C., Nasser, I.A., Popov, Y., Cunniff, J.C., Lundasen, T., et al., 2014. Fibroblast growth factor 21 limits lipotoxicity by promoting hepatic fatty acid activation in mice on methionine and choline-deficient diets. Gastroenterology 147:1073–1083 e1076.
[44] Itagaki, H., Shimizu, K., Morikawa, S., Ogawa, K., Ezaki, T., 2013. Morphological and functional characterization of non-alcoholic fatty liver disease induced by a methionine-choline-deficient diet in C57BL/6 mice. International Journal of Clinical and Experimental Pathology 6:2683–2696.
[45] Nasimian, A., Taheripak, G., Gorgani-Firuzjaee, S., Sadeghi, A., Meshkani, R., 2013. Protein tyrosine phosphatase 1B (PTP1B) modulates palmitate-induced cytokine production in macrophage cells. Inflammation Research : Official Journal of the European Histamine Research Society [et al] 62:239–246.
[46] Xiao, F., Waldrop, S.L., Bronk, S.F., Gores, G.J., Davis, L.S., Kilic, G., 2015. Lipoapoptosis induced by saturated free fatty acids stimulates monocyte migration: a novel role for Pannexin1 in liver cells. Purinergic Signalling 11: 347–359.
[47] Syn, W.K., Oo, Y.H., Pereira, T.A., Karaca, G.F., Jung, Y., Omenetti, A., et al., 2010. Accumulation of natural killer T cells in progressive nonalcoholic fatty liver disease. Hepatology 51:1998–2007.
[48] Pelz, S., Stock, P., Bruckner, S., Christ, B., 2012. A methionine-choline-deficient diet elicits NASH in the immunodeficient mouse featuring a model for hepatic cell transplantation. Experimental Cell Research 318:276–287.
[49] Haj, F.G., Markova, B., Klaman, L.D., Bohmer, F.D., Neel, B.G., 2003. Regulation of receptor tyrosine kinase signaling by protein tyrosine phosphatase-1B. Journal of Biological Chemistry 278:739–744.
[50] Escriva, F., Gonzalez-Rodriguez, A., Fernandez-Millan, E., Rondinone, C.M., Alvarez, C., Valverde, A.M., 2010. PTP1B deficiency enhances liver growth during suckling by increasing the expression of insulin-like growth factor-I. Journal of Cell Physiology 225:214–222.
[51] Takase, H.M., Itoh, T., Ino, S., Wang, T., Koji, T., Akira, S., et al., 2013. FGF7 is a functional niche signal required for stimulation of adult liver progenitor cells that support liver regeneration. Genes and Development 27:169–181.
[52] Lukacs-Kornek, V., Lammert, F., 2017. The progenitor cell dilemma: cellular and functional heterogeneity in assistance or escalation of liver injury. Journal of Hepatology 66:619–630.
[53] Awan, S.J., Baig, M.T., Yaqub, F., Tayyeb, A., Ali, G., 2017. In vitro differentiated hepatic oval-like cells enhance hepatic regeneration in CCl4-induced hepatic injury. Cell Biology International 41:51–61.
[54] de Lima, V.M., Oliveira, C.P., Alves, V.A., Chammas, M.C., Oliveira, E.P., Stefano, J.T., et al., 2008. A rodent model of NASH with cirrhosis, oval cell proliferation and hepatocellular carcinoma. Journal of Hepatology 49: 1055–1061.
[55] Michalopoulos, G.K., 2017. Hepatostat: liver regeneration and normal liver tissue maintenance. Hepatology 65:1384–1392.

